RSC Advances

ROYAL SOCIETY OF CHEMISTRY

www.rsc.org/advances

Interfacial self-assembly of nanoporous C_{60} thin films

Jean-Nicolas Tisserant,[†]* Patrick A. Reissner,[†] Sandra Jenatsch,[♮] Hannes Beyer,[†]

Roland Hany,[♮] Andreas Stemmer[†]*

[†]ETH Zürich, Nanotechnology Group, Säumerstrasse 4, CH-8803 Rüschlikon, Switzerland

[♮]Empa, Swiss Federal Laboratories for Materials Science and Technology,

Laboratory for Functional Polymers, Überlandstrasse 129, CH-8600 Dübendorf, Switzerland

Corresponding Authors

*jeanti@ethz.ch. * astemmer@ethz.ch

[†]ETH Zürich, Nanotechnology Group, Säumerstrasse 4, CH-8803 Rüschlikon, Switzerland

Abstract

Nanoporous surface morphologies often perform better than their planar or bulk counterparts in phenomena such as catalysis and charge transport. In organic photovoltaics, for example, fullerene films structured on a scale corresponding to the exciton diffusion length, typically a few ten nanometers, could improve charge separation. Existing methods to form such films, however, typically do not reach features smaller than 100 nm. Here, we propose a simple method based on interfacial

nucleation-and-growth to produce large and flexible 2D percolating assemblies of C_{60} nanoparticles with diameters below 50 nm that cover up to 60% of the surface. These films can be rendered insoluble by photo-polymerization and infiltrated with other functional molecules. We illustrate the benefit of such stabilized nanoporous films on the example of organic solar cells of the architecture ITO/TiO$_2$/C$_{60}$/P3HT/MoO$_3$/Ag. Structured C_{60} films with interconnected morphological features perform better than planar C_{60} films by 50% on average, reaching a power conversion efficiency of 1.3%. Due to the ease of film fabrication and small dimensions of the C_{60} morphological features, these results may find application beyond organic photovoltaics, in a variety of fields where enhanced interface with a fullerene surface is needed.

Keywords: Fullerene, nanostructure, solar cell, self-assembly, porous material, surface enhancement.

Introduction

Properties of nanomaterials in general, and porous materials in particular, differ from those of their bulk counterparts because surface and interface phenomena play an important role on the nanometer scale.[1] Enhanced interfaces compared to planar counterparts increase the efficiency of nanoporous materials in processes like catalysis,[2] gas storage,[3] molecular recognition,[4] separation,[5] and solar energy conversion. [6,7]

Carbon-rich materials such as fullerenes have played a fundamental role in the development of modern nanoscience and technology.[8,9] Nanoporous C_{60} films are for example used in catalytic methanol oxidation[10] or as electrode materials in aqueous solutions.[11] Beyond these two examples, the outstanding opto-electronic properties of

C_{60} associated with a versatile chemistry makes fullerenes interesting for optics[12] or biology[13] and essential for the entire organic photovoltaic (OPV) field where fullerenes are widely used as electron acceptor materials.[14–18] For such an application, nanoporous C_{60} thin films would be highly desirable because excitons are split into free charge carriers at molecular heterojunctions.[7] In many cases, active materials have been deposited as bilayers,[14,15,19,20] or interdigitated heterojunctions, usually using soluble fullerene derivatives[21–23] rather than pristine C_{60}.[24] Nanoporous C_{60} films with morphological features in the range of the typical exciton diffusion length, ~ 10-20 nm in comparable systems,[16,25,26] would offer an attractive alternative to bilayers in bi-component systems that do not phase-separate spontaneously to form an optimal bulk heterojunction morphology.

The fabrication of porous two-dimensional films of fullerenes on a large scale remains challenging. Some attempts were made by sacrificial templating,[27] electrodeposition from colloids,[28,29] or self-assembly of synthesized C_{60} nanoparticles.[30] These methods remain limited by the difficulty to prepare C_{60} nanopartices smaller than 100 nm in diameter.[30–32] Interfacial self-assembly has emerged as a promising method for the fabrication of free-floating films that can be readily integrated into functional devices.[33,34] In particular, progress in the field of metallic nanoparticle assembly[35] inspired the interfacial technique that we present here to form single-layer or multilayer two-dimensional C_{60} films having morphological features below 50 nm in diameter. Rapid solvent evaporation on an air/water interface is responsible for the formation of 2D interdigitated networks, typical of diffusion-limited colloid aggregation (DLCA).[36] The increase of interface area resulting from these nanostructures exceeds 30%. Importantly, the films are

floating on a liquid surface and are flexible, allowing further transfer onto any substrate.

Pristine C_{60} is known to photo-polymerize in the solid state in a 2+2 cycloaddition process.[37–40] This polymerization has for example been used to pattern fullerene films,[41] but was also identified as a degradation pathway that limits long term OPV cell performance.[40,42] Here, we use C_{60} photopolymerization to stabilize optimal fullerene morphologies against further solvent processing, similarly to results obtained by chemically modifying the fullerene.[26,43–45] Nanoporous films were stabilized, infiltrated with a well-known electron-donor material, poly(3-hexylthiophene-2,5-diyl) (P3HT) - resulting in finely inter-peretrating C_{60}/P3HT domains - and implemented as photoactive layer in C_{60}/P3HT solar cells. By adding a nanoporous C_{60} layer to the bilayer configuration, the enhanced interface and the film morphology adapted to the exciton diffusion length resulted in an improvement of 50% on average and up to 80% in the power conversion efficiency (PCE), reaching η=1.3%.

Experimental

Formation of C_{60} films. 5 mg of C_{60} (Aldrich, 99.9%) were ground to fine powder in a 5 mL glass vial. 5 mL of chloroform (Sigma Aldrich, > 99.8%) were added, the mixture was sonicated 30 minutes and left overnight to settle. C_{60} films were formed at the interface between water and air, in a 10 mL round poly(tetrafluoroethylene) (PTFE) beaker with a diameter of 2.1 cm by pouring dropwise 5 to 500 μL of saturated C_{60} solution on the convex water meniscus formed upon contact with PTFE. The films formed a thin brown and immobile layer on top of the water meniscus within a few minutes. Optionally, the C_{60} solution was deposited under reduced

pressure. If not stated otherwise, 50 μL of solution were deposited at a pressure of 500 mbar. To upscale the film area to several cm^2 for solar cell fabrication on 2.5x2.5 cm^2 large substrates, 100 μL of saturated C_{60} solution were deposited drop wise in a 3.8 cm wide PTFE beaker without applying vacuum.

Transfer to substrate. The films were transferred to Si/SiO_2 or glass by dipping the substrate vertically in the beaker and retracting it through the floating film. No double layers were formed by this process. To form multilayers, the same substrate was dipped and retracted through multiple freshly assembled films.

Stabilization and infiltration. C_{60} films were stabilized by light exposure (1 sun) overnight under inert atmosphere, at least 6h are necessary according to previously published results.[40] The solubility of stabilized films was tested by spin-coating (1000 rpm, 60 s) pure chloroform (1 mL on 4 cm^2). Regioregular P3HT (Rieke Speciality Polymers) was dissolved in chloroform (1.25 to 10 mg/mL) and spin-coated (1000 rpm, 30 s) on stabilized C_{60} films.

Solar cell fabrication. Except for nanoporous C_{60} film deposition, all device fabrication steps were done in a glove box under nitrogen (H_2O < 1 ppm, O_2 < 10 ppm). ITO substrates (Geomatec, sheet resistance 20 Ohms $square^{-1}$) were cleaned and coated with TiO_2 (50 nm).[46] To this end, 0.95 g of $Ti-(O-iC_3H_7)_4$ (Aldrich, 99.9%) were diluted in 10 mL of ethanol and stirred at 0°C. A solution consisting of concentrated HCl. (Sigma-Aldrich 0.03 g), water (0.135 g) and ethanol (10 mL) was added while stirring. The mixture was stirred 30 min at 0°C before spin-coating (step 1: 5 s, 300 rpm/s to 1000 rpm; step 2: 60 s, 3000 rpm/s, 4000 rpm). The films were annealed to 460°C in 3 h, kept at 460°C for 2 h, and cooled to room temperature. TiO_2 films were heated to 120°C on a hot plate under nitrogen (10 min) before depositing

any further layer. C_{60} nanostructured films were deposited on TiO_2 directly or on a 30 nm thick evaporated C_{60} layer. The films were dried on a hotplate (80°C) for 6 h under nitrogen to remove water and exposed to 1 sun illumination overnight under nitrogen to photo-polymerize C_{60}.[40] Planar C_{60} films were deposited by thermal evaporation at $< 5x10^{-6}$ mbar. The active layer was covered with 10 nm of thermally evaporated MoO_3 (Sigma Aldrich, 99.99%) as a buffer layer and 70 nm of Ag (Cerac, 99.99%) as an electrode. The active area of the cells was 0.031 or 0.071 cm^2.

Characterization. Scanning electron microscopy (SEM) was performed on a Hitachi SU8000 at a typical voltage of 1.5 kV. Images were analyzed using ImageJ. To evaluate lateral dimensions of the assemblies, SEM images of 1.2x1.2 μm^2 were binarized using an Otsu threshold. The line plot of such an image shows maxima at the averaged position of interfaces. Scanning force microscopy (SFM) was performed on an MFP-3D (Asylum Research) with Olympus AC160TS-R3 cantilevers. TEM was performed on a Philips CM30 operated at a voltage of 300 kV. Devices were transferred into an air-tight transfer box for *J–V* characteristics measurement under a solar simulator delivering a light intensity of 100 mW/cm^2. Photoluminescence was measured on a Fluorolog (Horiba Jobin-Yvon).

Results & discussion

Nanoporous C_{60} thin films

Two-dimensional nanostructured thin films of C_{60} were formed by evaporation of C_{60}-saturated chloroform solutions at the convex interface formed between water and air in a PTFE beaker (Figure 1a). The films obtained are percolating networks of C_{60} particles forming a single layer (Figure 1b), covering surfaces up to several square centimeters. A 400 μm^2 area is shown in Figure S1, Supplementary Information. The

films are floating on the water meniscus, allowing their transfer onto diverse substrates including glass, silicon, or metals. An example of a single layer 2D film deposited on silicon is shown in Figure 1b, c. Multilayer nanoporous films could be produced by successive deposition of films on the same surface (Figure 1d). The nanoporous films exhibit astonishing mechanical flexibility and can, for example, effectively cover pronounced geometrical kinks (Figure S2, Supplementary Information). This flexibility can be explained by the film morphology. SFM revealed that the C_{60} film is composed of agglomerated nanoparticles (Figure 2a, b). The typical height of the C_{60} particles is 20-30 nm (Figure 2c). The total C_{60} surface coverage reached up to 60%. Transmission electron microscopy (TEM) showed that the films are indeed composites of crystalline C_{60} nanoparticles between 10 and 50 nm bound together by amorphous C_{60} (Figure S3, Supplementary Information). The film shown in Figure 2 has a 36% increased surface area compared to a plain C_{60} film, considering the C_{60} particles as spheres.

A similar convex interface was already used to self-assemble 2D films of metallic nanoparticles.[35] Dushkin *et al.* measured and modeled the self-assembly of latex particles on water meniscus.[47] They found that latex colloidal crystals nucleate at the center of the meniscus and grow radially under capillary action until they cover most of the surface. This comparison, along with our morphological observations allows us to interpret the C_{60} film formation as follows: As the chloroform solution is suddenly brought into supersaturation under solvent evaporation, multiple nucleation events occur at the air/solvent interface. The mobile C_{60} clusters thus formed may in parallel either grow radially or aggregate on other clusters, forming morphologies typical of diffusion-limited colloid aggregation with multiple seeds.[36] This model was

tested by varying the amount of solution deposited on the water meniscus and the

surrounding pressure.
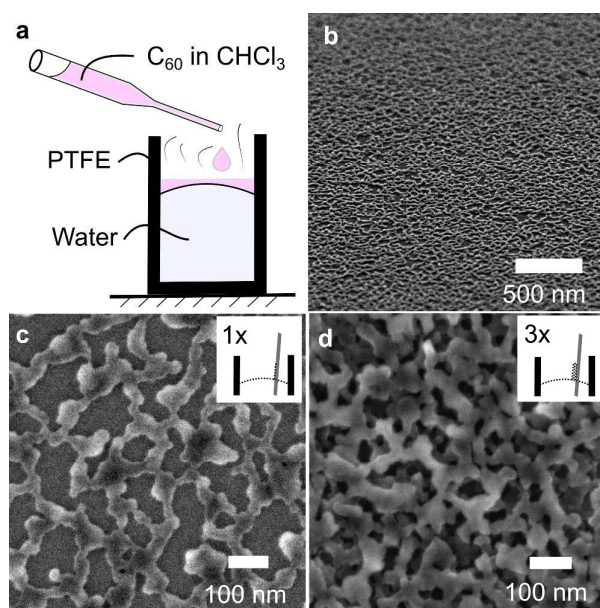
Figure 1. Fabrication of nanoporous C_{60} films. (a) Sketch of experimental setup

comprising a saturated C_{60} / $CHCl_3$ solution and water as the subphase in a PTFE

beaker; optionally, vacuum was applied around the beaker to tune the film

morphology; (b, c) SEM images of a single-layer C_{60} film); (d) SEM image of a triple

layer C_{60} film.
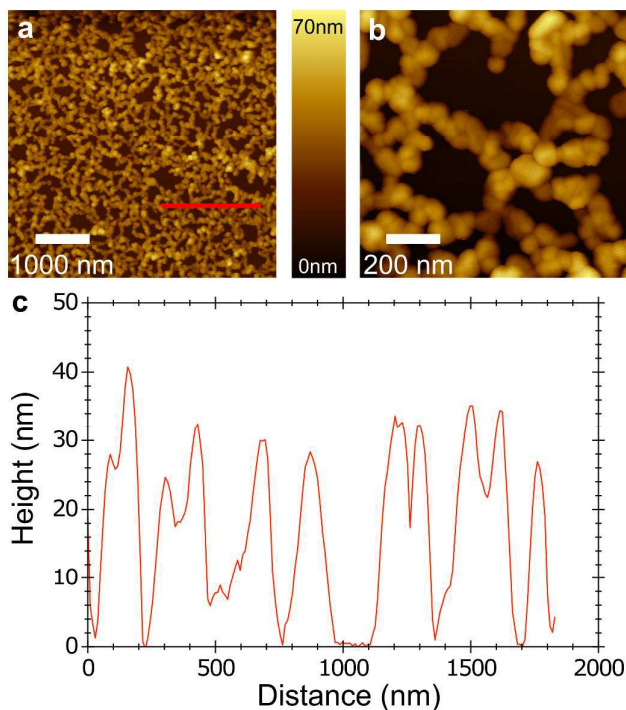
Figure 2. SFM characterization of a nanoporous C_{60} film. (a) 25 μm^2 scan showing 2D percolating structures typical of DLCA; (b) 1 μm^2 zoom showing that the film is composed of C_{60} nanoparticles with an average diameter of 32±10 nm; (c) profile plot extracted from (a) along the red line.

Tuneable film properties

Varying the volume of C_{60} solution deposited on the water meniscus allows tuning the total surface coverage with little variations of the lateral dimensions of the C_{60} structures (Figure 3a). The surface coverage could be varied between 37% and 60% by depositing 25 to 200 µL of C_{60}-saturated chloroform solution on 3.5 cm^2 of interface (Figure 3a). Below 25 µL, the film only partially covered the water meniscus. Above 250 µL, large C_{60} crystals formed at the air/water interface, leading to film inhomogeneity and no increased coverage (Figure S4, Supplementary Information). In order to probe the effect of solvent evaporation time, 50 µL of

saturated chloroform were deposited under pressures varying from 300 to 1000 mbar (Figure 3b). The surface coverage did not vary during this experiment. Lowering the surrounding pressure leads to the formation of smaller lateral dimensions of the assemblies, reaching 35 nm at 300 mbar. The lower pressure limit is given by the boiling point of the carrier liquid water. In summary, C_{60} coverage is mainly controlled by the volume of deposited solution, *i.e.* the number of nucleation events per unit surface, and the size of the resulting features is mainly controlled by the particle growth time, when solution and stable nuclei coexist. These two parameters, evaporation time and volume of deposited C_{60} solution allow tuning the morphological outcome of C_{60} thin films self-assembled on an air/water interface. The method was scaled up for film sizes over 11 cm^2 (see experimental section). Films obtained on such a large scale showed particles that were smaller than 25 nm with a surface coverage above 50% (Figure 4).
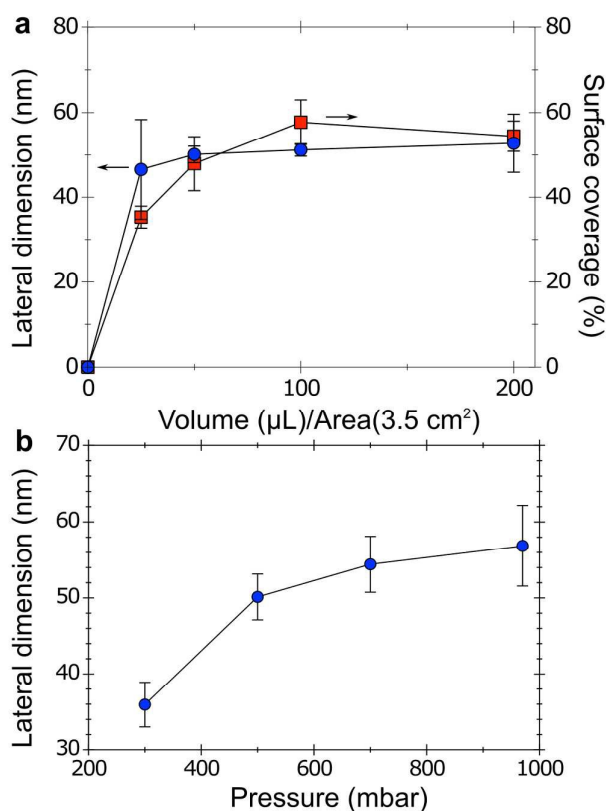
Figure 3. Evolution of the film morphology with experimental parameters. (a) Effect of the volume of deposited C_{60} solution on the lateral dimensions of C_{60} features and on the total surface coverage; (b) effect of the chamber pressure on the lateral dimensions of the C_{60} features (drop volume 50 μL in either case).

Morphology stabilization and P3HT infiltration

For the versatile use of nanostructured C_{60} films, the ability to freeze their optimal morphology against further processing or ageing is appealing.[26,43–45] It is known that C_{60} photo-polymerizes in the solid state, yielding poorly soluble species.[40] This reaction is used here to stabilize nanoporous C_{60} films against solvent processing. Solvent rinsing was carried out in a way that mimics the conditions under which films were treated during solar cell processing. The insolubility of flat polymerized C_{60} films reached almost 100% (Figure 4a, b). For nano-structured C60 films, SFM measurements (Figure 4c-e) of the same area before and after solvent rinsing showed an overall insolubility of 84±15% (average of 5 samples). A reference SEM image demonstrating the pronounced solubility of a C_{60} film that was not polymerized is shown in Figure S5, Supplementary Information. We found a similar level of stability against solvent rinsing for as-prepared films, and for films used for solar cell fabrication that were annealed and dried before photo-stabilization.

The insolubility of stabilized nanoporous C_{60} films allows infiltrating them with a second material from the same casting solvent. P3HT coated from chloroform was taken as an example to illustrate the concept (see Figure S6, Supplementary Information). The concentration of P3HT was optimized to completely cover the C_{60} nanostructures. The peak-to-valley amplitude was reduced from 72 nm to 3.3 nm by increasing the P3HT concentration up to 10 mg/mL. Films coated at 5 mg/mL

resulted in an optimal morphology and were chosen for the rest of the study. High-resolution SFM (see Figure S7, Supplementary Information) and SEM (Figure 5) were used to prove that P3HT chains effectively infiltrate the nanoscopic voids in C_{60} films.
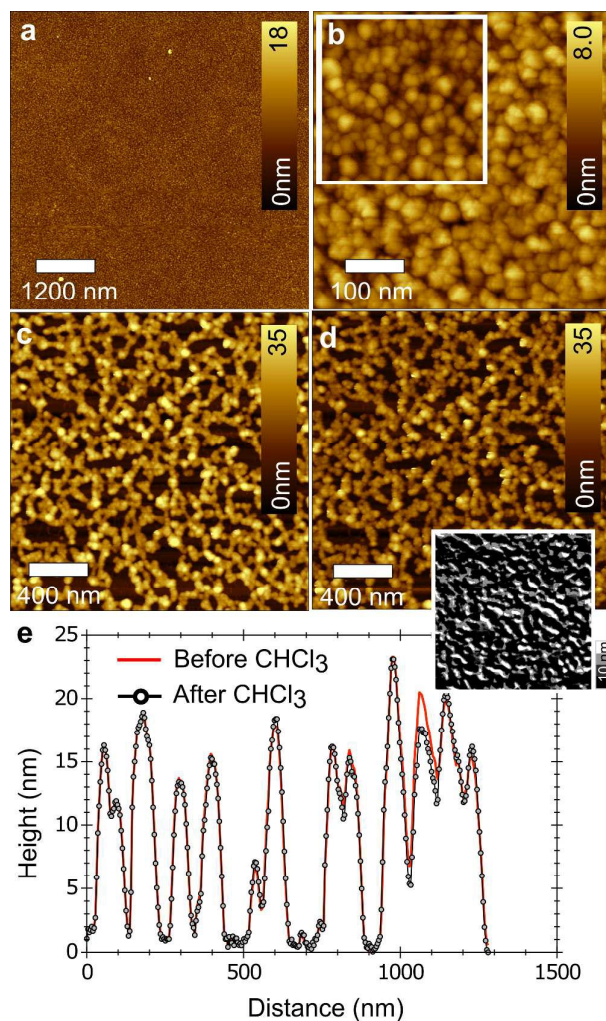
Figure 4. Stabilization of the C_{60} nanoporous morphology on glass against solvent rinsing. (a) Flat C_{60} after photo-polymerization and solvent rinsing; (b) 500 nm large zoom of the same sample, the inset shows a flat C_{60} film directly after deposition; (c) nanostructured C_{60} film after photo-polymerization and before solvent rinsing; (d)

same area imaged after solvent rinsing, the inset maps the difference in height between (c) and (d); (e) representative profiles extracted from (c) and (d).

Use in solar cells

The merits of a C_{60} small-scale stabilized particle network can be demonstrated *via* improved charge separation in organic photovoltaics.[7] Devices with the configuration $ITO/TiO_2/C_{60}/P3HT/MoO_3/Ag$ were fabricated to measure the effect of C_{60} nano-morphology on cell performance. The C_{60} layer was either flat (40 nm evaporated C_{60}, named F-C_{60}), or nanostructured as described above (S-C_{60}) or a stack of both structures, S-C_{60} on 30 nm F-C_{60}. 30 nm F-C_{60} films were chosen in this case to keep the film absorption constant. Removing water from S-C_{60} films before illumination was done by thermally annealing the samples under nitrogen (6 h, 80°C). Drying induced a slight coarsening of the morphology. The change in morphology and the insolubility of films that were dried on a hotplate before polymerization are shown in Figure S8, Supplementary Information. Solar cell performance data are summarized in Table 1. First, C_{60} stabilization was essential to device performance as pristine C_{60} is largely dissolved when attempting to infiltrate P3HT from a chloroform solution. Consequently, the performance of non-stabilized F-C_{60}/P3HT cells was poor (Table 1, entry a). Stabilized F-C_{60}/P3HT cells reached on average $\eta = 0.67\%$ with J_{SC} = 2.5 mA/cm^2, $V_{OC} = 0.48$V, $FF = 56.8\%$ (Table 1, entry b). S-C_{60} alone, even when stabilized, performed less than F-C_{60} (Table 1, entry c and d). This can be ascribed to the lower electron acceptor content in a S-C_{60} film, as compared to F-C_{60}, and P3HT contacting directly the TiO_2 layer. These two adverse effects were reduced by

stacking two S-C_{60} layers on top of each other (Table 1, entry e), and suppressed by depositing S-C_{60} on top of F-C_{60} (Table 1, entry f). In the latter case, and for a constant total cell absorption, the average cell performance was increased by ~50% compared to the flat film. Adding a further S-C_{60} layer increased the best device performance further (Table 1, entry g).

Table 1. Summary of solar cell performance data.

Entry	Structure of C_{60} layer	V_{OC} [V]	J_{SC} [mA cm^{-2}]	FF [%]	η [%]	η_{max} [%]
a	F-C_{60} no light	0.29 (0.10)	1.3 (0.4)	29.6 (9.5)	0.13 (0.1)	0.27
b	F-C_{60} light	0.48 (0.02)	2.5 (0.2)	56.8 (2.3)	0.67 (0.1)	0.71
c	1 layer S-C_{60} no light	0.16 (0.04)	0.43 (0.1)	30.8 (3.0)	0.02 (0.01)	0.03
d	1 layer S-C_{60} light	0.42 (0.08)	0.92 (0.3)	45.9 (5.8)	0.18 (0.1)	0.27
e	2 layers S-C_{60} light	0.48 (0.02)	1.50 (0.7)	46.4 (2.2)	0.32 (0.1)	0.41
f	1 layer S-C_{60} on F-C_{60} light	0.52 (0.004)	3.3 (0.3)	59.0 (1.6)	1.0 (0.1)	1.14
g	2 layers S-C_{60} on F-C_{60} light	0.47 (0.09)	3.4 (0.9)	53.2 (5.4)	0.87 (0.3)	1.28

F-C_{60} denotes a planar C_{60} film, S-C_{60} a nanostructured film. Solar cell performance parameters are the average and standard deviation (s.d) values of a batch of more than 11 identically processed devices. V_{OC} denotes the open-circuit voltage, J_{SC} the short-circuit current, FF the fill factor, and η the power conversion efficiency.

Cross-section SEM images of S-C_{60} and S-C_{60} on F-C_{60} active layers are shown in Figure 5a, b, respectively, and a cross-section SEM image of F-C_{60} active layer is shown in Figure S9, Supplementary Information. The SEM images reveal an enhanced interface after adding S-C_{60} on F-C_{60}. From SFM data shown earlier, an increase of the interface area of ~18% can be calculated by considering each C_{60}

feature as half-spherical, and the interface increase is about 36% for spherical structures. From this, it is clear that the 50% average increase in the cell efficiency and in particular the 32% increase in J_{SC} upon adding one S-C_{60} layer onto F-C_{60} is mainly due to an increase of the C_{60}/P3HT interface. This hypothesis is also supported by photoluminescence experiments. The difference between P3HT emission on F-C_{60} and on S-C_{60} / F-C_{60} is close to 30% (Figure S10, Supplementary Information). Internal photon-to-current conversion efficiency (IPCE) data from F-C_{60} and 2 x S-C_{60} on F-C_{60} devices are shown in Figure S11, Supplementary Information. The IPCE maximum value was 30% for F-C_{60} and 42% for 2 x S-C_{60} on F-C_{60}.

Reports on C_{60}/P3HT solar cells are scarce, because of the low solubility of C_{60} in organic solvents and because the two components do not spontaneously phase-separate to form an optimal bulk-heterojunction morphology, limiting drastically the cell performance.[24] One solution found by Geiser *et al.* was to anneal the whole device to force the morphology to evolve favorably, reaching over 2% in PCE.[24] Even if the final PCE shown here does not reach that of bulk-heterojunction fullerene/P3HT devices, the solution proposed, using a C_{60} film stabilized in an optimal morphology, can be seen as rather universal and opens important improvement possibilities for other working systems.
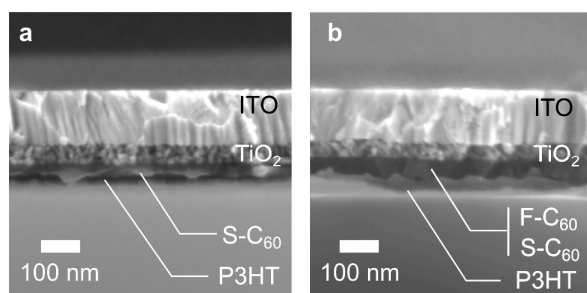
Figure 5. Use of nanoporous C_{60} films (S-C_{60}) in solar cells. (a) SEM cross-section image of the S-C_{60} cell without top contact; (b) SEM cross section of the S-C_{60} / F-C_{60} cell.

Conclusions

In this article we have shown a new method based on interfacial nucleation-and-growth to form nanoporous C_{60} films. They can be described as 2D percolating networks of C_{60} nanoparticles with diameters below 50 nm and as small as 10 nm. The particles are the smallest and most monodisperse reported to date. Both single-layer and multilayer films could be readily fabricated, stabilized against further solvent processing, and the process was up-scaled to several square centimeters. The lateral dimensions of C_{60} domains below 50 nm make such thin film morphologies highly adapted for any physical or chemical process where an enhanced interface is advantageous. We chose to illustrate this by the example of increased performance in organic P3HT-based solar cells, accomplished by an enhanced C_{60}/P3HT interface and adapted donor/acceptor morphology. However, we believe that our assembly method may be extended beyond fullerenes and OPV, to other functional molecules and fields where enhanced interface matters, such as catalysis, sensing or fuel cells.

Acknowledgments

Electronic Supplementary Information (ESI) available: SEM images of large area nanostructured C_{60} films, SEM images of S-C_{60} deposited on a 90° geometric kink, a TEM image of S-C_{60}, an SEM image of large C_{60} crystals, SEM images showing the solubility of S-C_{60} films that were not illuminated, SFM images of P3HT infiltration, an SFM study of S-C_{60} films upon drying, an SEM side-image of a F-C_{60}/P3HT solar cell, P3HT photoluminescence data, and IPCE measurements of characteristic solar cells.

References

1   A. Zangwill, *Physics at Surfaces*, Cambridge University Press, Cambridge, UK, 1988.

2   H. L. Ngo and W. Lin, *Top. Catal.*, 2005, **34**, 85–92.

3   H. Furukawa and O. M. Yaghi, *J. Am. Chem. Soc.*, 2009, **131**, 8875–83.

4   D. Bonifazi, S. Mohnani and A. Llanes-Pallas, *Chemistry*, 2009, **15**, 7004–25.

5   Q. Min Wang, D. Shen, M. Bülow, M. Ling Lau, S. Deng, F. R. Fitch, N. O. Lemcoff and J. Semanscin, *Microporous Mesoporous Mater.*, 2002, **55**, 217–230.

6   J. Burschka, N. Pellet, S.-J. Moon, R. Humphry-Baker, P. Gao, M. K. Nazeeruddin and M. Grätzel, *Nature*, 2013, **499**, 316–9.

7   S. E. Gledhill, B. Scott and B. A. Gregg, *J. Mater. Res.*, 2011, **20**, 3167–3179.

8   H. W. Kroto, A. W. Allaf and S. P. Balm, *Chem. Rev.*, 1991, **91**, 1213–1235.

9   J. M. Ball, H. W. Paul and T. D. Anthopoulos, in *Advances in Carbon Nanomaterials: Science and Applications*, ed. N. Tagmatarchis, Pan Stanford Publishing Pte. Ltd., 2012, vol. 78, pp. 978–981.

10   K. Vinodgopal, M. Haria, D. Meisel and P. Kamat, *Nano Lett.*, 2004, **4**, 415–

418.

11   A. Szucs, A. Loix, J. B. Nagy and L. Lamberts, *Synth. Met.*, 1996, **77**, 227–230.

12   X. L. Jenekhe, S. A.; Chen, *Science*, 1999, **283**, 372–375.

13   A. W. Jensen, S. R. Wilson and D. I. Schuster, *Bioorg. Med. Chem.*, 1996, **4**, 767–779.

14   N. S. Sariciftci, D. Braun, C. Zhang, V. I. Srdanov, A. J. Heeger, G. Stucky and F. Wudl, *Appl. Phys. Lett.*, 1993, **62**, 585.

15   G. Yu, J. Gao, J. C. Hummelen, F. Wudl and A. J. Heeger, *Science*, 1995, **270**, 1789–1791.

16   P. Peumans, A. Yakimov and S. R. Forrest, *J. Appl. Phys.*, 2003, **93**, 3693.

17   A. W. Hains, Z. Liang, M. A. Woodhouse and B. A. Gregg, *Chem. Rev.*, 2010, **110**, 6689–735.

18   H. Spanggaard and F. C. Krebs, *Sol. Energy Mater. Sol. Cells*, 2004, **83**, 125–146.

19   C. W. Tang, *Appl. Phys. Lett.*, 1986, **48**, 183.

20   J. J. M. Halls, K. Pichler, R. H. Friend, S. C. Moratti and A. B. Holmes, *Appl. Phys. Lett.*, 1996, **68**, 3120.

21   F. Yang, M. Shtein and S. R. Forrest, *Nat. Mater.*, 2004, **4**, 37–41.

22   M. Granström, K. Petritsch, A. C. Arias, A. Lux, M. R. Andersson and R. H. Friend, *Nature*, 1998, **395**, 257–260.

23   J. Xue, B. P. Rand, S. Uchida and S. R. Forrest, *Adv. Mater.*, 2005, **17**, 66–71.

24   A. Geiser, B. Fan, H. Benmansour, F. Castro, J. Heier, B. Keller, K. E. Mayerhofer, F. Nüesch and R. Hany, *Sol. Energy Mater. Sol. Cells*, 2008, **92**, 464–473.

25   H. Hoppe and N. S. Sariciftci, *J. Mater. Chem.*, 2006, **16**, 45–61.

26   D. E. Markov, E. Amsterdam, P. W. M. Blom, A. B. Sieval and J. C. Hummelen, *J. Phys. Chem. A*, 2005, **109**, 5266–74.

27   J. Heier, R. Steiger, F. Nüesch and R. Hany, *Langmuir*, 2010, **26**, 3955–61.

28   S. Barazzouk, S. Hotchandani and P. V. Kamat, *Adv. Mater.*, 2001, **13**, 1614–1617.

29   H.-G. Jeon, S. Ryo, T. Sugiyama, I. Oh, H. Masuhara and T. Asahi, *Chem. Lett.*, 2007, **36**, 1160–1161.

30   R. Kudo, J. Matsui, T. Yokoyama, A. Masuhara, H. Kasai, H. Oikawa and T. Miyashita, *Mol. Cryst. Liq. Cryst.*, 2011, **539**, 408–412.

31   S. Deguchi, R. G. Alargova and K. Tsujii, *Langmuir*, 2001, **17**, 6013–6017.

32   R. G. Alargova, S. Deguchi and K. Tsujii, *J. Am. Chem. Soc.*, 2001, **123**, 10460–10467.

33   X. Ye, J. E. Collins, Y. Kang, J. Chen, D. T. N. Chen, A. G. Yodh and C. B. Murray, *Proc. Natl. Acad. Sci. U. S. A.*, 2010, **107**, 22430–5.

34   X. Ye, J. Chen, M. Engel, J. A. Millan, W. Li, L. Qi, G. Xing, J. E. Collins, C. R. Kagan, J. Li, S. C. Glotzer and C. B. Murray, *Nat. Chem.*, 2013, **5**, 466–73.

35   V. Santhanam, J. Liu, R. Agarwal and R. P. Andres, *Langmuir*, 2003, **19**, 7881–7887.

36   M. Y. Lin, H. M. Lindsay, D. A. Weitz, R. C. Ball, R. Klein and P. Meakin, *Nature*, 1989, **339**, 360–362.

37   P. C. Eklund, A. M. Rao, P. Zhou, Y. Wang and J. M. Holden, *Thin Solid Films*, 1995, **257**, 185–203.

38   A. M. Rao, P. Zhou, K. A. Wang, G. T. Hager, J. M. Holden, Y. Wang, W. T. Lee, X. X. Bi, P. C. Eklund, D. S. Cornett, M. A. Duncan and I. J. Amster, *Science*, 1993, **259**, 955–957.

39   M. Suzuki, T. Iida and K. Nasu, *Phys. Rev. B - Condens. Matter Mater. Phys.*, 2000, **61**, 2188–2198.

40   H. Zhang, A. Borgschulte, F. A. Castro, R. Crockett, A. C. Gerecke, O. Deniz, J. Heier, S. Jenatsch, F. Nüesch, C. Sanchez-Sanchez, A. Zoladek-Lemanczyk and R. Hany, *Adv. Energy Mater.*, 2015, **5**, 1400734.

41   J. Wang, C. Larsen, T. Wågberg and L. Edman, *Adv. Funct. Mater.*, 2011, **21**, 3723–3728.

42   G. Wicht, S. Bücheler, M. Dietrich, T. Jäger, F. Nüesch, T. Offermans, J.-N. Tisserant, L. Wang, H. Zhang and R. Hany, *Sol. Energy Mater. Sol. Cells*, 2013, **117**, 585–591.

43   J.-F. Nierengarten and S. Setayesh, *New J. Chem.*, 2006, **30**, 313.

44   J.-N. Tisserant, R. Hany, E. Wimmer, A. Sánchez-Ferrer, J. Adamcik, G. Wicht, F. Nüesch, D. Rentsch, A. Borgschulte, R. Mezzenga and J. Heier, *Macromolecules*, 2014, **47**, 721–728.

45   M. Drees, H. Hoppe, C. Winder, H. Neugebauer, N. S. Sariciftci, W. Schwinger, F. Schäffler, C. Topf, M. C. Scharber, Z. Zhu and R. Gaudiana, *J. Mater. Chem.*, 2005, **15**, 5158.

46   E. Berner, T. Jäger, T. Lanz, F. Nüesch, J.-N. Tisserant, G. Wicht, H. Zhang and R. Hany, *Appl. Phys. Lett.*, 2013, **102**, 183903.

47   C. D. Dushkin, G. S. Lazarov, S. N. Kotsev, H. Yoshimura and K. Nagayama, *Colloid Polym. Sci.*, 1999, **277**, 914–930.

Graphical abstract:

Enhanced interface   *Functionality*
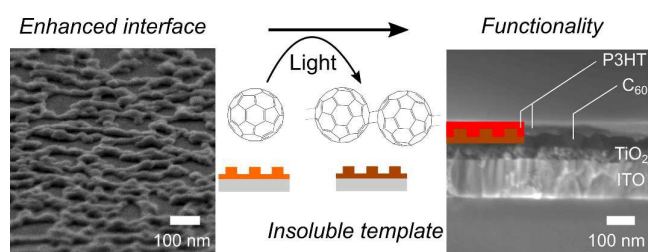
Self-assembled stabilized nanoporous C_{60} films offer an enhanced active interfacial area.